Global galactic dynamo driven by cosmic rays and exploding magnetized stars

Michał Hanasz, Dominik Wóltański, Kacper Kowalik

ABSTRACT

We report first results of first global galactic-scale CR-MHD simulations of cosmic-ray-driven dynamo. We investigate the dynamics of magnetized interstellar medium (ISM), which is dynamically coupled with the cosmic-ray (CR) gas. We assume that exploding stars deposit small-scale, randomly oriented, dipolar magnetic fields into the differentially rotating ISM, together with a portion of cosmic rays, accelerated in supernova shocks. We conduct numerical simulations with the aid of a new parallel MHD code PIERNIK. We find that the initial magnetization of galactic disks by exploding magnetized stars forms favorable conditions for the cosmic-ray-driven dynamo. We demonstrate that dipolar magnetic fields supplied on small supernova remnant scales can be amplified exponentially by the CR-driven dynamo, to the present equipartition values, and transformed simultaneously to large galactic scales. The resulting magnetic field structure in an evolved galaxy appears spiral in the face-on view and reveals the so-called X-shaped structure in the edge-on view.

Subject headings: galaxies: ISM — galaxies: magnetic fields — cosmic rays — ISM: magnetic fields — MHD

1. Introduction

It is commonly believed that galactic magnetic fields are generated by a kind of dynamo process. Dynamos require, however seed fields. Various cosmological processes have been considered as candidates for the seed field generation mechanisms, such as phase transitions in the early universe, and battery effects on protogalactic scales. However, known processes of this kind lead to weak fields of the order of 10^{-20} G (see Widrow 2002).

Another possibility, suggested by Syrovatskii (1970), developed by Bisnovatyi-Kogan, Ruzmaikin, & Syunyaev (1973), and by Rees (1987, 2006), is that the seed fields may have been created during early stages of galactic evolution by a stellar-scale Biermann battery, subsequently amplified by stellar dynamos, and then spread into the interstellar medium (ISM) by stellar explosions. Rees (1987) estimates that a contribution of 10^6 Crab-type, randomly oriented plerionic supernova remnants may lead to 10^{-9} G mean magnetic field on galactic scales.

---

[1]Centre for Astronomy, Nicholas Copernicus University, PL-87148 Piwnice/Toruń, Poland; mhanasz@astri.uni.torun.pl

In a series of recent papers (Hanasz et al. 2004, 2006, 2009b), we have shown that in local, shearing-box MHD simulations, weak magnetic fields can be amplified up to a few µG within $1 - 2$ Gyr, by the dynamo process driven by buoyancy of cosmic rays, as proposed by Parker (1992). The aim of this paper is to demonstrate that small-scale, randomly oriented, dipolar magnetic fields of stellar origin, can be amplified in a similar rate, and regularized by the cosmic-ray-driven dynamo in global galactic disk CR–MHD simulations.

Global model of the CR-driven dynamo

To built up a global galactic disk model, we use the realistic Milky Way gravitational potential by Allen & Santillan (1991). We neglect, however, the galactic bulge contribution, to obtain smoother rotation curve near the galactic center. Without the bulge contribution rotational velocity approaches $V_\phi \simeq 220$ km/s at the galactocentric radius of Sun. The initial setup for the gaseous disk, supernova rate, and its spatial distribution is based on the global ISM model by Ferriere (1998).

The global model of CR-driven dynamo involves the following elements, introduced previously in the local models: (1) the cosmic ray component – a relativistic gas described by the diffusion–advection transport equation, supplemented to the standard set of resistive MHD equations. (2) Cosmic rays supplied in supernova remnants. The cosmic ray input of individual SNe is assumed 10% of the typical SN kinetic energy output ($= 10^{51}$ erg), while the thermal energy output from supernovae is neglected. (3) Following Giacalone & Jokipii (1999), we assume that CRs diffuse anisotropically along magnetic field lines. (4) We incorporate a finite resistivity of the ISM, to permit topological evolution of galactic magnetic fields via anomalous resistivity processes (see Hanasz et al. 2002, and references therein), and/or via turbulent reconnection (Kowal et al. 2009), on small spatial scales, which are unresolved in our simulations. (5) Differential rotation of the interstellar gas, which currently follows the assumed form of galactic gravitational potential.

Moreover, contrary to our previous models, we assume that (6) no magnetic field is present in the initial configuration, and that a weak, randomly oriented, dipolar magnetic field is supplied in 10 % of supernova remnants.

2. Numerical setup

We use the PIERNIK MHD code (Hanasz et al. 2010a,d), which is a grid-MHD code based on the Relaxing TVD (RTVD) scheme by Jin & Xin (1995) and Pen, Arras, & Wong (2003). PIERNIK is parallelized by means of block decomposition with the aid of MPI library. The original scheme is extended to deal with dynamically independent, but interacting fluids: thermal gas and a diffusive cosmic ray gas, described within the fluid approximation (Hanasz et al. 2010b). The code has been equipped with the resistivity module (Hanasz et al. 2010c). The induction equation, including
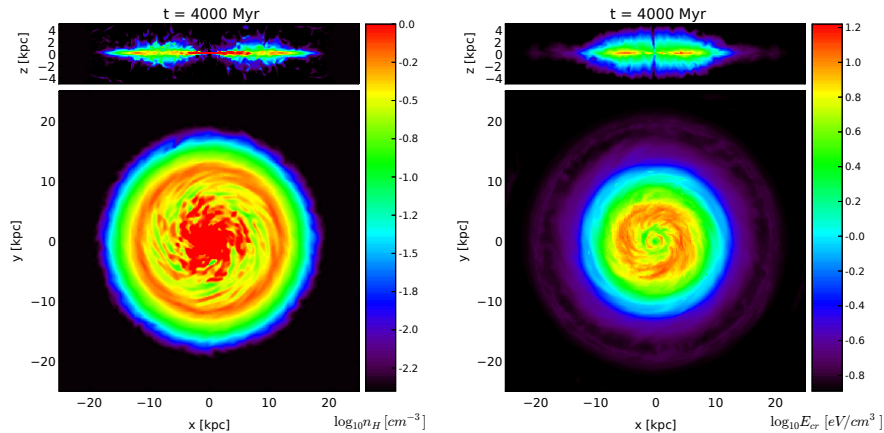
Fig. 1.— Logarithm of gas number density in units of hydrogen atom per cubic centimeter (left) and cosmic ray energy density distribution in units of electron volt per cubic centimeter (right) at $t = 4$ Gyr.

the Ohmic resistivity term, is integrated with the aid of the constraint transport (CT) algorithm (Evans & Hawley 1988).

The CR diffusion algorithm follows the implementation of CR transport described by Hanasz & Lesch (2003). The CR diffusion–advection equation is integrated in a conservative manner. The CR anisotropic diffusion is parameterized by parallel and perpendicular (with respect to the local magnetic field direction) diffusion coefficients $K_\parallel$ and $K_\perp$. We assume that CRs couple to gas through the CR pressure gradient term in the gas equation of motion (see Berezinskii et al. 1990).

The simulation presented here has been performed with the resolution of $500 \times 500 \times 100$ grid cells, distributed in $10 \times 10 \times 2$ equal size MPI blocks, in the Cartesian domain spanning the volume 50 kpc $\times$ 50 kpc $\times$ 10 kpc in x, y and z directions respectively. Initial gas distribution represents a hydrostatic equilibrium state for gas column density given by Ferriere (1998). The probability distribution for occurrence of SN remnants, derived from Ferriere (1998) was fixed over simulation time. Magnetic vector potential of a single SNR is computed, following Jackson (1999) for a current-loop of a radius comparable to the radius of SNR (50 pc in the present model). We stop the dipolar magnetic field input after 1 Gyr of the disk evolution, because the corresponding procedure is computationally expensive, while the contribution of the supplied dipoles becomes negligible with respect to dynamo amplification dominating at later times. The values of diffusion coefficients adopted for the present simulation are $K_\parallel = 3 \times 10^{28}$ cm^2 s^{-1} and $K_\perp = 3 \times 10^{26}$ cm^2 s^{-1} (see Strong et al. 2007, and references therein for a more extensive discussion on CR diffusion). In the present model we assume a uniform magnetic diffusivity $\eta = 3 \cdot 10^{24}$ cm^2 s^{-1}, and neglect heating of the thermal gas by resistive dissipation of magnetic fields. We apply outflow boundary conditions on upper and lower domain boundaries, and enforce gas to follow the prescribed rotation curve outside the outer disk radius $r_{\max} = 21.5$ kpc. To prevent significant mass losses, due to the CR-driven

wind, we re-supply into the disk the gas lost from the computational domain.

3. Results

3.1. Structure of ISM

The gas density distribution and cosmic ray energy distribution in the disk are displayed in vertical and horizontal slices through the disk center, for $t = 4\,\mathrm{Gyr}$, in Figure 1, while the distribution of toroidal magnetic field component is shown for four different epochs in Figure 2.

The gas and cosmic ray distributions achieve dynamical equilibrium in about 100 Myr of initial SN activity. The characteristic shape of the disk, apparent in the gas and CR distributions, reflects the initial ring-like structure of the gaseous disk. Vertical wind blowing with the speed exceeding $100\,\mathrm{km\ s^{-1}}$, apparently above and below the central part of the disk, carries out the gas component at the overall rate of $1 M_\odot$ per year.

3.2. Amplification and Structure of Magnetic Field

Magnetic field amplification originating from the small-scale, randomly oriented dipolar magnetic fields is apparent through the exponential growth, by several orders of magnitude, of both the magnetic flux and magnetic energy, as displayed in Figure 3. The growth phase of magnetic field starts at the beginning of the simulation, initially via a quick accumulation of magnetic energy of the supplied magnetic dipoles. The growth of magnetic field strength saturates at about $t = 4\,\mathrm{Gyr}$, reaching values $3 - 5\,\mathrm{\mu G}$ in the disk. During the amplification phase, magnetic flux and total magnetic energy grow by about 6 and 10 orders of magnitude, respectively. As is remarkable in Figure 3, the growth in the magnetic flux magnitude is close to exponential. The average e-folding time of magnetic flux is approximately equal 270 Myr, corresponding to the rotation at galactocentric radius equal approximately 10 kpc. During the initial period ending at $t = 2.3\,\mathrm{Gyr}$, magnetic flux changes sign and its absolute value variates randomly around the exponential curve. These variations are associated with the evolving magnetic field structure shown in Figure 2. Magnetic field initially is entirely random, at $t = 20\,\mathrm{Myr}$, since it originates from randomly oriented magnetic dipoles. Later on the toroidal magnetic field component forms a spiral structure revealing reversals in the disk plane, as is apparent at $t = 700\,\mathrm{Myr}$. Magnetic field structure evolves gradually toward larger and lager scales. The toroidal magnetic field direction becomes almost uniform inside the disk around $t = 2.5\,\mathrm{Gyr}$, when the total magnetic flux stops to reverse in Figure 3. The domination of fluctuating magnetic field, during the transformation phase of magnetic structure, is apparent also through the excess of the total magnetic energy above the exponential curve. The volume occupied by the well-ordered magnetic field expands continuously till the end of the simulation.

Magnetic field reveals a spiral structure, as shown in the face-on views, and expansion of the

unidirectionally magnetized disk toward larger galactocentric radii is apparent in the edge-on views. The latter effect seems to reflect the overall outflow geometry. Observation of gas and magnetic field fluctuations moving through the computational domain (in animated images corresponding to vertical slices in Figure 2) reveals a superposition of vertical thickening combined with radial expansion in outer parts of the disk.

We note magnetic field reversals apparent at $t = 700$Myr and $t = 2500$Myr, where the central part of the disk toroidal magnetic field has opposite polarity with respect to the remaining part of the disk. In the snapshot corresponding to $t = 4800$Myr, the toroidal magnetic field is almost unidirectional in the horizontal cut through the galactic midplane, but displays a clear reversal in the vertical slice. The apparent magnetic field configuration comprises two regions of opposite polarity of toroidal magnetic field, therefore, one reversal remains till the end of the simulation. In a more extensive set of simulations we have done till now, the uniformity of final magnetic field configurations and the number of reversals depends, among other parameters, on the CR diffusion coefficients, which are known only to an order of magnitude accuracy. If the parallel CR-diffusion coefficient is reduced by an order of magnitude with respect to the value used in the presented simulation, magnetic field structure, observed over the period of several Gyr, resembles to that presented in Figure 2 for $t = 700$Myr.

To visualize the magnetic field structure in a manner resembling to radio observations of external galaxies, we construct synthetic radio maps of synchrotron radio-emission, using IDL package by Wiatr (2006). We apply standard procedures of integration of stokes parameters I, Q, and U for the polarized synchrotron emissivity, along the line of sight (see e.g. Rohlfs 1986; Longair 1994). To compute synchrotron emissivity, we use magnetic field vectors and CR energy distribution. In the computations of synthetic radio maps, we assume that the ratio of CR electron energy density to CR proton energy density is 0.01, the maximum and minimum energies of cosmic ray protons are 10^9 and 10^{15}eV, respectively, and the power index of CR spectrum is 2.3. We neglect the effects of synchrotron cooling of CR electrons, and the effects of Faraday rotation.

In Figure 4, we show the polarized intensity of synchrotron emission (color maps) together with polarization vectors. Electric vectors, computed on the basis of integrated Stokes parameters are rotated by 90°, to reproduce the magnetic field direction averaged along the line of sight, under the assumption of vanishing Faraday rotation effects. The polarization vectors, indicating the mean magnetic field direction, reveal a regular spiral structure in the face-on view, and the so-called *X-shaped structure* in the edge-on view. This kind of structures are presented in radio maps of real galaxies (Soida 2005; Krause et al. 2006; Krause 2009), and have been investigated recently in terms of CR-driven dynamo by Otmianowska-Mazur et al. (2009). A particular similarity can be noticed between our edge-on synthetic radio map and the radio maps of the edge-on galaxies NGC 891 (Krause 2009) and NGC 253 (Heesen et al. 2009). In the present global model, the X-shaped configuration is an intrinsic property of the magnetic field structure, since it corresponds closely to the X-shaped distribution of magnetic field in the disk and its neighborhood, as shown in Figure 2.

4. Discussion and conclusions

We have shown that the Cosmic-Ray driven dynamo experiment conducted for a whole galactic disk, seeded by small-scale magnetic dipoles and cosmic rays supplied in supernova remnants, amplifies magnetic fields exponentially, up to the equipartition level, and develops large-scale magnetic fields in the disk and the surrounding galactic halo. The amplification timescale of the large-scale magnetic field component is close to the disk rotation period, i.e., 270 Myr for the present simulation. The initially disordered magnetic field contributions from randomly oriented magnetic dipoles are efficiently ordered within the first 2 Gyr of disk evolution. The presented experiment supports strongly the idea that galactic dynamos may have been initiated by small-scale magnetic fields of stellar origin.

We note, finally, that the present model requires further development, since in the present version the underlying gravitational potential is axisymmetric. Preliminary results obtained for simulations with spiral arms indicate the possibility that reversals are related to the spiral structure in gravitational potential. Our present model indicates the possibility of efficient action of CR-driven dynamo, but is still too preliminary to be confronted directly with observational data of a particular galaxy such as Milky Way. Therefore, incorporation of the effects of spiral arms is needed for a more detailed confrontation of our model with the observational results suggesting existence of magnetic field reversals (see Han & Zhang 2007, and references therein) and magnetic arms (e.g. Beck 2007).

REFERENCES

Allen, C., & Santillan, A. 1991, Rev. Mex. Astron. Astrofis., 22, 255

Beck, R. 2007, A&A, 470, 539

Berezinskii, V. S., Bulanov, S. V., Dogiel, V. A., & Ptuskin, V. S. 1990, Astrophysics of Cosmic Rays (Amsterdam: North-Holland, 1990, edited by Ginzburg, V.L.)

Bisnovatyi-Kogan, G. S., Ruzmaikin, A. A., & Syunyaev, R. A. 1973, Sov. Astron., 17, 137

Evans, C. R., & Hawley, J. F. 1988, ApJ, 332, 659

Ferriere, K. 1998, ApJ, 497, 759

Giacalone, J., & Jokipii, J. R. 1999, ApJ, 520, 204

Han, J. L., & Zhang, J. S. 2007, A&A, 464, 609

Hanasz, M., Kowal, G., Otmianowska-Mazur, K., & Lesch, H. 2004, ApJ, 605, L33

Hanasz, M., Kowalik, K., Wóltański, D., & Pawłaszek, R. 2010a, in Proc. Extra-Solar Planets in Multi-Body Systems, ed. K. Goździewski, A. Niedzielski, J. Schneider, EAS Conf. Series, EDP Sciences, (in press, arXiv:0812.2161)

—. 2010b, in Proc. Role of Disk-Halo Interaction in Galaxy Evolution: Outflow vs. Infall?, ed. M. de Avillez, EAS Conf. Series, EDP Sciences, (in press, arXiv:0812.4839)

—. 2010c, in Proc. Role of Disk-Halo Interaction in Galaxy Evolution: Outflow vs. Infall?, ed. M. de Avillez, EAS Conf. Series, EDP Sciences, (in press, arXiv:0901.0104)

Hanasz, M., Kowalik, K., Wóltański, D., Pawłaszek, R., & Kornet, K. 2010d, in Proc. Extra-Solar Planets in Multi-Body Systems, ed. K. Goździewski, A. Niedzielski, J. Schneider, EAS Conf. Series, EDP Sciences, (in press, arXiv:0812.2799)

Hanasz, M., & Lesch, H. 2003, A&A, 412, 331

Hanasz, M., Otmianowska-Mazur, K., Kowal, G., & Lesch, H. 2006, Astron. Nachr., 327, 469

—. 2009b, A&A, 498, 335

Hanasz, M., Otmianowska-Mazur, K., & Lesch, H. 2002, A&A, 386, 347

Heesen, V., Krause, M., Beck, R., & Dettmar, R. 2009, (in press, arXiv:0908.2985)

Jackson, J. D. 1999, Classical Electrodynamics (3rd ed.; New York: Wiley)

Jin, S., & Xin, Z. 1995, Commun. Pure Appl. Math., 48, 235

Kowal, G., Lazarian, A., Vishniac, E. T., & Otmianowska-Mazur, K. 2009, ApJ, 700, 63

Krause, M. 2009, Rev. Mex. Astron. Astrofis., 36, 25

Krause, M., Wielebinski, R., & Dumke, M. 2006, A&A, 448, 133

Longair, M. S. 1994, High Energy Astrophysics. Vol. 2. Stars, the Galaxy and the Interstellar Medium. (Cambridge: Cambridge University Press)

Otmianowska-Mazur, K., Soida, M., Kulesza-Żydzik, B., Hanasz, M., & Kowal, G. 2009, ApJ, 693, 1

Parker, E. N. 1992, ApJ, 401, 137

Pen, U.-L., Arras, P., & Wong, S. 2003, ApJS, 149, 447

Rees, M. J. 1987, QJRAS, 28, 197

—. 2006, Astron. Nachr., 327, 395

Rohlfs, K. 1986, Tools of Radio Astronomy (Berlin: Springer)

Soida, M. 2005, in The Magnetized Plasma in Galaxy Evolution, ed. K. T. Chyzy, K. Otmianowska-Mazur, M. Soida, & R.-J. Dettmar, (Kraków: Jagiellonian Univ.), 185

Strong, A. W., Moskalenko, I. V., & Ptuskin, V. S. 2007, Annu. Rev. Nucl. Part. Sci., 57, 285

Syrovatskii, S. 1970, in Interstellar Gas Dynamics, ed. H. Habing, IAU Symp. 39, Dordrecht, Holland, D. Reidel Pub. Co., 192

Wiatr, R. 2006, MSc thesis, Nicolaus Copernicus Univ.
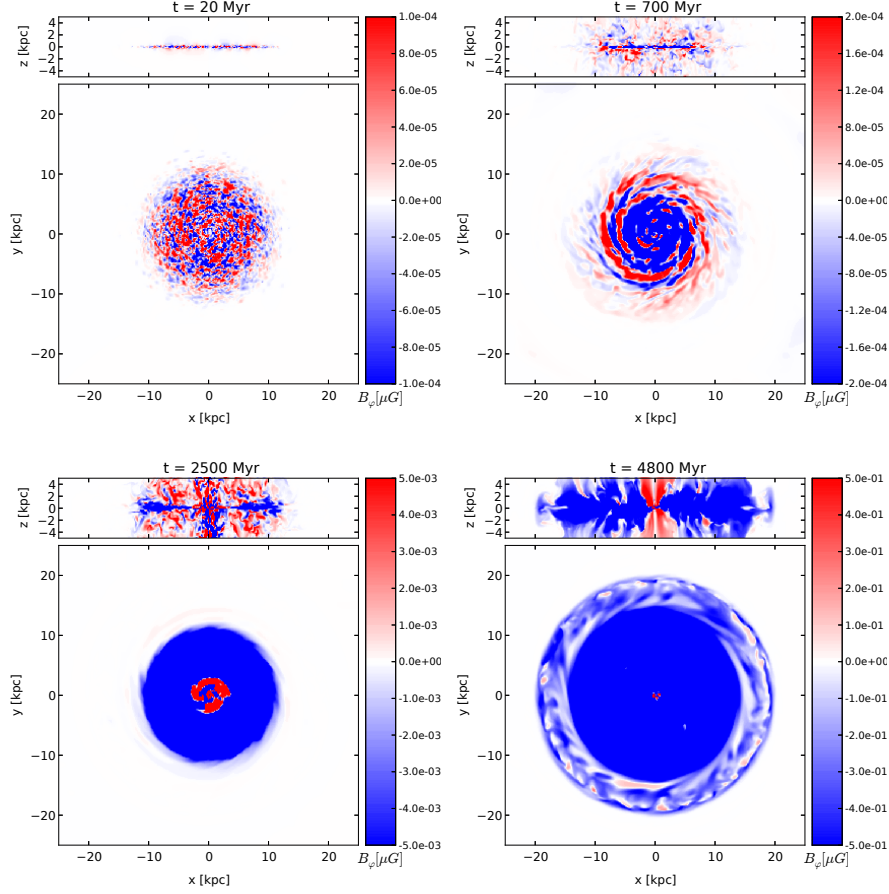
Widrow, L. M. 2002, Rev. Mod. Phys., 74, 775

Fig. 2.— Distribution of toroidal magnetic field at $t = 20\,$Myr (top left), $t = 700\,$Myr (top right), $t = 2.5\,$Gyr (bottom left), and $t = 4.8\,$Gyr (bottom right). Unmagnetized regions of the volume are white, while positive and negative toroidal magnetic fields are marked with red and blue, respectively. Note that the color scale in magnetic field maps is saturated to enhance weaker magnetic field structures in disk peripheries. The maximum magnetic field strengths are $5.9 \cdot 10^{-4}$, $4.4 \cdot 10^{-3}$, 1.5, and 29 μG at $t = 0.02, 0.7, 2.5,$ and 4.8Gyr, respectively.
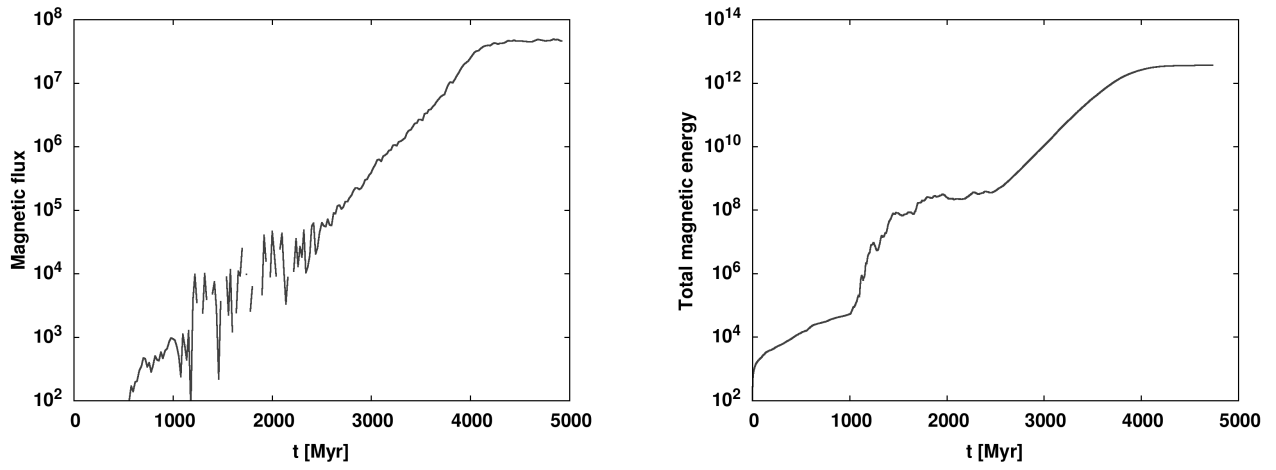
Fig. 3.— Temporal evolution of toroidal magnetic flux and total magnetic energy in scaled units. The final saturation level corresponds to the equipartition magnetic fields.
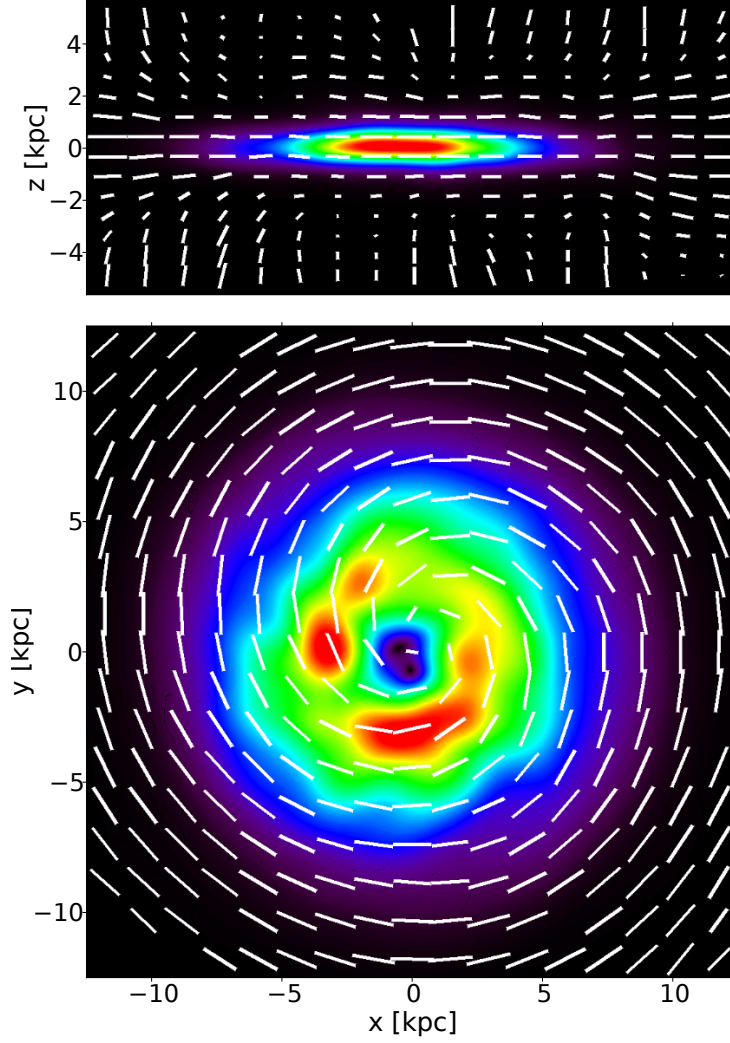
Fig. 4.— Synthetic radio maps of polarized intensity (PI) of synchrotron emission, together with polarization vectors are shown for the edge-on and face-on views of the galaxy at $t = 4.8$ Myr. Vectors direction resembles electric vectors rotated by 90°, and their lengths are proportional to the degree of polarization.